Application of the bounds-analysis approach to arsenic and gallium antisite defects in gallium arsenide

A. F. Wright and N. A. Modine

Phys. Rev. B **91**, 014110 — Published 23 January 2015

DOI: 10.1103/PhysRevB.91.014110

Application of the bounds-analysis approach to arsenic and gallium antisite defects in gallium arsenide

A. F. Wright and N. A. Modine

Sandia National Laboratories, Albuquerque, New Mexico 87185-1415, USA

ABSTRACT

A recently developed bounds-analysis approach has been used to interpret density-functional-theory (DFT) results for the As and Ga antisites in GaAs. The bounds analysis and subsequent processing of DFT results for the As antisite yielded levels - defined as the Fermi levels at which the defect charge state changes - in very good agreement with measurements, including the −1/0 level which is within 0.1 eV of the conduction-band edge. Good agreement was also obtained for the activation energies to transform the As_{Ga} from its metastable state to its stable state. For the Ga antisite, the bounds analysis revealed that the −1 and 0 charge states are hole states weakly bound to a localized −2 charge state. The calculated levels are in good agreement with measurements.

I. INTRODUCTION

Point defects in semiconductors typically exist in more than one charge state. The charge states of a defect and its levels, which are defined as the Fermi levels at which the charge state changes, are technologically important because they control the relative rates of carrier capture and emission, and thus determine how much influence a defect has on the performance of a minority-carrier device. Since experimental studies of defects are challenging, there has been considerable interest in theoretical defect studies.

Theoretical studies of point defects rely mainly on Kohn-Sham density-functional theory [1] (DFT) and a semilocal exchange-correlation functional such as the local density approximation (LDA) [2] or generalized gradient approximation (GGA). [3] DFT calculations are typically performed in a periodically repeated parallelpiped (*supercell*) containing a single defect surrounded by bulk material. Candidate charge states are simulated by adding electrons to or removing electrons from the defect supercell, and DFT is used to minimize the supercell energies of the candidate charge states with respect to their ionic coordinates. The results are then analyzed to identify the stable defect charge states and processed to enable comparisons with experimental data and modeling of the defect's influence on minority-carrier devices. [4]

In this study, DFT has been used to determine the charge states and levels of the As antisite (As_{Ga}) and Ga antisite (Ga_{As}) in GaAs. Details about the DFT calculations, the identification of the As_{Ga} and Ga_{As} charge states, and the processing of the levels associated with these charge states are described in Section II. A novel aspect of this study is the use of a recently developed *bounds-analysis approach* [5] to identify and

interpret the DFT results for the candidate As_{Ga} and Ga_{As} charge states. In Section III, the charge states and levels of As_{Ga} and Ga_{As} are reported and compared with measurements and previous theoretical results. In addition, activation energies for thermal transitions between two different As_{Ga} structures are reported and compared with measurements.

II. THEORETICAL TECHNIQUES

A. DFT calculations

Kohn-Sham DFT calculations were performed using the Socorro code, [6] with periodic boundary conditions, a plane wave basis, [7] norm-conserving pseudopotentials (NCPs), [8] and LDA [2] exchange and correlation. Semilocal Ga^{+3} and As^{+5} NCPs were constructed using the FHI98PP code [9] and converted into local potentials and Kleinman-Bylander projectors [10] for use in Socorro. A 40 Ryd energy cutoff was used to define the plane-wave basis set for the Kohn-Sham orbitals and Kleinman-Bylander projectors, and a 160 Ryd cutoff was used to define the plane-wave basis set for the electron density and local potentials. The occupations of the Kohn-Sham orbitals were calculated from their eigenvalues using a Fermi function with $kT = 0.0257$ eV, and Brillouin-zone sampling meshes (denoted $n \times n \times n$, where n is an integer) were constructed using the Monkhorst-Pack technique. [11]

To validate the NCPs, equilibrium lattice parameters were determined for bulk gallium, arsenic, and GaAs. DFT calculations for zinc-blende GaAs were performed in 2-atom primitive supercells with seven lattice constants ranging from 5.451 Å to 5.768 Å

and using 5×5×5 sampling meshes. The supercell energies were fit using the Murnaghan equation, [12] which yielded an equilibrium lattice constant of 5.607 Å and a bulk modulus of 0.721 Mbar. A subsequent calculation at the equilibrium lattice constant yielded a direct Kohn-Sham band gap of 0.70 eV. Consistent with general trends found when using the LDA, the lattice constant is 0.8% smaller than measured value (5.653 Å), [13] the bulk modulus is 4.8% larger than measured value (0.756 Mbar), [14] and the Kohn-Sham band gap, $\Delta_{KS} = 0.70$ eV, is less than half of the measured gap at low temperature (1.52 eV). [15] DFT calculations for bulk gallium were performed for an orthorhombic *A*11 structure using a 24×24×24 sampling mesh. The equilibrium lattice constants were a = 4.440 Å, b = 4.454 Å, and c = 7.524 Å, which are 1.5% smaller than measured values. [16] Calculations for bulk arsenic were performed for a rhombohedral *A*7 structure also using a 24×24×24 sampling mesh. The hexagonally-transformed equilibrium lattice constants were a = 3.741 Å and c = 10.131 Å, which are 0.5% and 3.0% smaller than measured values. [17]

Candidate charge states were chosen for each defect type as discussed in Section III. The charge states were simulated by adding electrons to or removing electrons from defect supercells formed by inserting various defect configurations reported in the literature into bulk supercells. The supercell energy was then minimized by relaxing the ionic coordinates of the supercell using DFT ionic forces. To test the stability of the relaxed structure, atoms near the defect were given small displacements and the energy was then minimized again. In all cases, the purturbed structure returned to the original relaxed structure. Since the periodic boundary conditions used in the DFT calculations produced an infinite periodic array of defects, a uniform compensating charge density

was added to supercells having non-zero charge states to obtain well-defined solutions to Poisson's equation.[18] Defect calculations were performed in cubic 216-, 512- and 1000-atom supercells with sizes L = 3×, 4× and 5×5.607 Å, where L is the cube root of the supercell volume. Uncertainties in the supercell energies due to Brillouin-zone sampling were reduced to 0.02 eV by using multiple sampling meshes: 2×2×2, 3×3×3, 4×4×4, and 5×5×5 in the 216-atom supercells; 2×2×2, 3×3×3, and 4×4×4 in the 512-atom supercells; and 2×2×2 and 3×3×3 in the 1000-atom supercells.

B. Analysis of candidate defect charge states

Due to the substantially reduced band gaps obtained in DFT calculations using semilocal functionals, a defect level that is experimentally observed to be in the band gap may lie within one of the band edges in the DFT calculation and therefore involve partial occupation of bulk conduction-band states or de-occupation of bulk valence-band states for one or both of its associated charge states.[5] In addition to introducing errors in the DFT levels, this can make it difficult to identify the defect charge states. To help mitigate this difficulty, we recently developed a bounds-analysis approach[5] to interpreting defect results from semilocal DFT calculations. The basis of this approach is a comparison of the DFT levels with bounds representing the energies to add an electron to and remove an electron from the bulk material in a defect supercell. To make this more precise, consider a defect of type D in a supercell of size L. The level associated with candidate charge states q and $q - 1$ is given by the equation[19, 20]

$$\Delta^D(q-1/q,L) = E^D(q-1,L) - E^D(q,L) - \varepsilon_{VBE}, \quad (1)$$

in which $E^D(q,L)$ and $E^D(q-1,L)$ are the supercell energies of the two charge states and the level is referred to the Kohn-Sham eigenvalue of bulk GaAs at the valence-band-edge (VBE), ε_{VBE}. (For future reference, we note that one can think of this level as arising from either the addition of an electron to a supercell in charge state q or the removal of an electron from a supercell in charge state $q-1$.) The upper bound is defined as the energy to add one electron to a neutral bulk supercell of size L,[5]

$$\Delta^B(-1,L) = E^B(-1,L) - E^B(0,L) - \varepsilon_{VBE}, \quad (2)$$

and the lower bound is defined as the energy to remove one electron from a neutral bulk supercell of size L,[5]

$$\Delta^B(+1,L) = E^B(0,L) - E^B(+1,L) - \varepsilon_{VBE}, \quad (3)$$

where $E^B(0,L)$ is the energy of the neutral bulk supercell, $E^B(-1,L)$ is the energy with one electron added, $E^B(+1,L)$ is the energy with one electron removed, and the bounds are referred to ε_{VBE} for consistency with the definition of a defect level (Eq. 1). Due to band-filling effects,[5] these bounds have substantial supercell-size dependences and the bounds analysis is facilitated by plotting the levels and bounds together vs. inverse supercell size $(1/L)$[21] and extending the bounds to the infinite supercell-size limit ($1/L$ =

0) via cubic-spline fits of the calculated bounds; $\Delta^{B,fit}(-1,L)$ and $\Delta^{B,fit}(+1,L)$. At this limit, $E^B(-1,L)-E^B(0,L)\to\varepsilon_{CBE}$, the Kohn-Sham eigenvalue of bulk GaAs at the conduction-band-edge (CBE), and the upper bound thus becomes $\varepsilon_{CBE}-\varepsilon_{VBE}=\Delta_{KS}$, the Kohn-Sham band gap.[5] Likewise, the lower bound becomes $\varepsilon_{VBE}-\varepsilon_{VBE}=0$. We refer to reader to Ref. 5 for further details about the bounds and how to efficiently calculate them in large supercells.

A bounds analysis was performed for each defect type and structure.[5] The first step in the analysis was to identify the defect charge states from among the candidate charge states. This was done for each supercell size (L) by a process of elimination. If the calculated level between two candidate charge states was at or above the upper bound, the more negative of the charge states was eliminated since it involves addition of an electron to bulk-like conduction-band states. Likewise, if the calculated level was at or below the lower bound, the more positive of the candidate charge states was eliminated since it involves removal of an electron from bulk-like valence-band states. If the level was between the lower and upper bounds, neither of the two candidates was eliminated.

In the second step, the supercell-size dependence of each defect level identified in the first step was inspected to see if the level was: (1) near a bound, and (2) followed the bound, i.e., maintained a constant energy separation from it as a function of the inverse supercell size. As noted in Ref. 5, these criteria indicate that at least one of the associated charge states may be a hydrogenic state having a charge distribution which is weakly-localized at the defect. The charge states associated with levels that did not meet these criteria were provisionally identified as having well localized charge distributions (subject to the third step in the analysis).

In the third step, the defect levels that did not meet the criteria in the second step were compared with the bounds at the infinite supercell-size limit (Δ_{KS} and 0). If the calculated level was above Δ_{KS}, the more negative charge state could involve partial occupation of delocalized bulk conduction-band states. Likewise, a negative calculated level indicates that the more positive charge state might involve partial de-occupation of delocalized bulk valence-band states. If the level was between the VBE and CBE, its charge states were identified as having well-localized charge distributions. For each defect charge state that was identified as having partial occupation or de-occupation of delocalized bulk states, the magnitude of the delocalized charge was estimated using a technique described in Ref. 5, in which the excess charge in a bulk supercell was varied until the Fermi level became equal to the Fermi level of the defect supercell. If the relative delocalized charge was less than 20%, the charge state was processed using the procedures described in the next section, recognizing that the results will be less reliable than results for charge states without delocalized charge. (The 20% criterion is not based on a rigorous analysis at this point, but rather on an observation that a 20% delocalization did not significantly alter the dilute limit of an As_{Ga} level as discussed in Section III.A.)

The bounds analysis thus identifies three types of defect states: (1) states with well-localized charge distributions, (2) states with partially localized and delocalized charge distributions, and (3) states that may have weakly-localized charge distributions characteristic of hydrogenic states. The first type is suitable for processing using the standard procedures described in the next section that are applicable to well-localized charge distributions. For the second type, the technique described in Ref. 5 is used to quantify the partial delocalization and determine if the state is suitable for processing

using the standard procedures discussed in the next section. For the third type, further analysis is needed to confirm that the state is truly hydrogenic. If this is so, then it is not suitable for processing using the standard procedures described in the next section. Since the bounds-analysis approach may be unfamiliar to some readers, we emphasize that it precedes and is separate from the processing discussed in the next section.

C. Processing defect supercell energies

For defect charge states having suitably localized charge distributions, we used standard procedures to process their supercell energies and thereby obtain results that can be compared with experimental data and theoretical results in the literature. To begin, we calculated the defect formation energies. For a defect with structure *D* in a supercell of size *L* with charge state *q*, the formation energy is given by the equation [22, 23, 24]

$$E_f^D\left(q,L,E_F\right)=E^D\left(q,L\right)-E^B\left(0,L\right)-\Sigma_i n_i\mu_i+qE_F, \tag{4}$$

in which $E^D\left(q,L\right)$ is the defect supercell energy and $E^B\left(0,L\right)$ is the energy of a neutral bulk supercell of size *L* obtained using the same sampling mesh as the defect supercell. The third term is a sum over the number of atoms, n_i, of type *i* that were added to $\left(n_i>0\right)$ and removed from $\left(n_i<0\right)$ a bulk supercell to form the defect structure, multiplied by the chemical potential, μ_i, of a reservoir providing atomic exchange. Therefore, this term is $\mu_{Ga}-\mu_{As}$ for As_{Ga} and $\mu_{As}-\mu_{Ga}$ for Ga_{As}. Our formation energies are reported for *As-rich conditions* in which μ_{As} is the DFT energy per atom of bulk *A*7

arsenic and $\mu_{Ga} = \mu_{GaAs} - \mu_{As}$, where μ_{GaAs} is the DFT energy per formula unit of bulk GaAs. The fourth term in Eq. 4 involves the Fermi level, E_F, which is defined in terms of the chemical potential of a reservoir providing electron exchange, μ_e, and a relative Fermi level, ε_F, such that $E_F = \mu_e + \varepsilon_F$. In this study, we used the customary convention in which μ_e is the Kohn-Sham eigenvalue at the VBE, ε_{VBE}.

Due to the use of periodic boundary, the formation energies obtained from Eq. 4 contain supercell-size-dependent electrostatic interactions that were removed by fitting the formation energies to the Makov-Payne formula [25] truncated at the third-order term,

$$E_f^{D,fit}\left(q,L,\varepsilon_{VBE}\right) = E_f^{D,fit}\left(q,L\to\infty,\varepsilon_{VBE}\right) - \frac{\alpha\left(q\,|e|\right)^2}{\varepsilon L} + \frac{A_3}{L^3}. \quad (5)$$

In this formula, $\alpha = 2.8373$ is the Madelung constant of a cubic lattice of point charges, $q\,|e|$, embedded in a uniform compensating background charge, *e* is the electron charge, $\varepsilon = 12.8$ is the static dielectric constant of GaAs, [26] and $E_f^{D,fit}\left(q,L\to\infty,\varepsilon_{VBE}\right)$ is the defect formation energy in the limit of an infinite-sized supercell (*the dilute limit*), which is obtained from the fit along with the parameter of the third-order term, A_3. From these fits, the supercell-size dependences (*ssd*) of the defect levels and their dilute limits were obtained from the equation [24]

$$\Delta^{D,ssd}\left(q-1/q,L\right) = E_f^{D,fit}\left(q-1,L,\varepsilon_{VBE}\right) - E_f^{D,fit}\left(q,L,\varepsilon_{VBE}\right), \quad (6)$$

which is analogous to Eq. 1 for this choice of the Fermi level $\left(E_F = \varepsilon_{VBE}\right)$. We note that to obtain a more compact presentation of our defect results, we will plot the supercell-size dependences of the defect levels, $\Delta^{D,ssd}\left(q-1/q,L\right)$, together with the DFT levels, $\Delta^{D}\left(q-1/q,L\right)$, and the cubic-spline fits of the defect bounds, $\Delta^{B,fit}\left(-1,L\right)$ and $\Delta^{B,fit}\left(+1,L\right)$. However, this presentation should not be taken to indicate that the bounds analysis depends on the fits of the defect levels. As noted above, the bounds analysis solely involves comparisons of the DFT levels, $\Delta^{D}\left(q-1/q,L\right)$, with the defect bounds.

To compare the dilute limits of the levels with measurements, the DFT VBE and CBE were shifted to align them with the measured VBE and CBE. In this study, the VBE shift, Δ_{VBE}, was chosen to be −0.41 eV so that the calculated +1/+2 level of As_{Ga} agrees with the measured +1/+2 level. A CBE shift, Δ_{CBE}, was then chosen so that $\Delta_{CBE} - \Delta_{VBE} = 0.82$ eV and the corrected DFT band gap agrees with the measured band gap at low temperature (1.52 eV). [15] We note that this procedure is analogous to the Marker Method [27] in that Δ_{VBE} is determined by aligning a DFT level with a measured level. It is also consistent with results from recent theoretical studies that compared levels obtained using semilocal functionals and hybrid functionals. [19, 28] These studies showed that semilocal and hybrid functionals give similar separations between defect levels, but the band edges from the hybrid functionals are shifted roughly equally toward lower (VBE) and higher (CBE) energies compared with the band edges from the semilocal functionals. For consistency with the shifts of the defect levels, we note that $q\Delta_{VBE}$ was added to the reported formation energies (Eq. 5).

III. RESULTS

A. As antisite charge states and levels

As_{Ga} is the defect that results when an As atom substitutes for a Ga atom in GaAs. From experimental and theoretical studies,[29] it has a stable state referred to as *EL*2 and a (higher-energy) metastable state referred to as *EL*2*. From experiments, *EL*2 is known to have T_d symmetry, three charge states (0, +1, +2), and two levels (+1/+2, 0/+1).[29] Deep-level transient spectroscopy measurements find the +1/+2 level 0.54 eV above the VBE and the 0/+1 level 0.77 eV above the VBE.[30] At temperatures below 140 K, neutral *EL*2 can be optically excited into neutral *EL*2*, which has C_{3v} symmetry.[29] DFT studies by two groups played an important role in establishing that *EL*2* forms when the substituted As atom shifts along a <1,1,1> direction into a planar configuration with three of its near-neighbor As atoms.[31, 32] From experiments, *EL*2* is known to have two charge states (−1, 0) and one level (−1/0) 0.016 eV above the CBE at ambient pressure.[33]

We began our studies of *EL*2 and *EL*2* by choosing candidate charge states, calculating their DFT energies and levels (Eq. 1), and performing a bounds analysis on the results. To illustrate the bounds analysis, we review the results from our earlier study of the *EL*2 levels[5] in which we considered the three observed charge states (0, +1, +2) plus two additional candidates (−1, +3). In Fig. 1, we plot the levels and cubic-spline fits of the bounds vs. inverse supercell size (1/*L*). From these plots, we eliminated the +3 charge state because the +2/+3 levels were at the lower bounds, and the −1 charge state because the −1/0 levels were above the upper bounds. Since the +1/+2 and 0/+1 levels

were between the bounds, we concluded that +2, +1, and 0 are *EL*2 charge states, in agreement with experimental results.[29] From an inspection of Fig. 1, we also concluded that the +1/+2 and 0/+1 defect levels do not involve partially occupied or de-occupied bulk states because the levels are between the 0 and Δ_{KS}. In addition, we concluded that the 0, +1, and +2 charge states are not hydrogenic since the levels are well-separated from the bounds and do not follow them.

Having identified the *EL*2 charge states, we processed them for comparison with measurements. The dashed lines in Fig. 1 are the supercell-size dependences of the defect levels, $\Delta^{D,ssd}(+1/+2,L)$ and $\Delta^{D,ssd}(0/+1,L)$. In the dilute limit, they yield a +1/+2 level 0.13 eV above the VBE and a 0/+1 level 0.36 eV above the VBE. After shifting the VBE by Δ_{VBE} (–0.41 eV), the 0/+1 level is 0.76 eV above the measured VBE in good agreement with the measurement of Lagowski *et. al.*[30] (0.77 eV) in *p*-type GaAs (see TABLE I). The formation energies at the dilute limit (including the $q\Delta_{VBE}$ shift) are 0.19 eV for the +2 charge state, 0.73 eV for the +1 charge state, and 1.49 eV for the 0 charge state (see TABLE II).

There have been numerous DFT studies of *EL*2, beginning in 1988 with the pioneering work of Dabrowski and Scheffler[31] and Chadi and Chang.[32] More recent studies include those of Schultz and von Lilienfeld in 2009,[34] Komsa and Pasquarello in 2011,[28] and Chroneos *et al*. in 2014.[35] Our levels are 0.05 eV higher than the levels obtained by Schultz and von Lilienfeld using the LDA, and the 0.22 eV difference between our levels is close to the 0.24 eV found by Schultz and von Lilienfeld.[34] Our 1.49 eV formation energy for neutral *EL*2 is likewise close to the 1.50 eV obtained by Schultz and von Lilienfeld,[34] and 0.26 eV higher than the formation energy found by

Chroneos *et al* in a 216-atom supercell. [35] The study of Komsa and Pasquarello [28] surveyed the effect of hybrid functionals, which combine exact and semilocal electronic exchange to reduce DFT band gap errors. Using theoretical GaAs lattice constant and functionals tuned to give a band gap in good agreement with measurements, Komsa and Pasquarello obtained a +1/+2 level 0.04 eV higher than the measurement and a 0/+1 level 0.2 eV higher than the measurement.

For *EL*2*, we began with the two observed charge states (−1, 0) and added three more candidates (−3, −2, +1). In Fig. 2, we plot the levels from these charge states and cubic-spline fits of the bounds vs. inverse supercell size. From an inspection of the plots, we eliminated the +1 and −3 charge states and concluded that −2, −1, and 0 are *EL*2* charge states. Since the −2/−1 and −1/0 levels do not follow the upper bound, we concluded that the −2, −1, and 0 charge states are not hydrogenic. However, the −2/−1 and −1/0 levels are above Δ_{KS}, indicating that the added electrons in the −1 and −2 charge states were partially delocalized in bulk conduction-band states. Specifically; 8, 15, and 22% of the first added charge was in bulk regions of the 216-, 512-, and 1000-atom supercells, and 25, 30, and 38% of the second added charge.

Given the sizeable bulk occupations in the −2 charge state, we concluded that the −2 charge state and the −2/−1 level would be better suited to consideration with hybrid functionals. Given the smaller bulk occupations in the −1 charge state, we processed the energies of the −1 and 0 charge states. The dashed line in Fig. 2 is the supercell-size dependence of the defect level, $\Delta^{D,ssd}(-1/0,L)$, which yields a dilute limit 1.05 eV above the VBE. After shifting the VBE by Δ_{VBE} and the CBE by Δ_{CBE}, the −1/0 level was found to be 1.46 eV above the measured VBE and thus 0.06 eV below the measured

CBE at low temperature. To test the sensitivity of this result to bulk occupations, we calculated the energies of the 0 and −1 charge states in a 64-atom supercell using a 7×7×7 sampling mesh for which the estimated bulk occupation of the added charge was 3%. Repeating the processing using energies from the 64-, 216-, and 512-atom supercells yielded a −1/0 level 0.02 eV lower than the level obtained above.

Our result for the −1/0 level is in good agreement with the measurements of Dreszer and Baj [33] who found the −1/0 level to be 0.016 eV above the CBE at ambient pressure (TABLE I). Our result is also in good agreement with a theoretical model proposed by Dabrowski and Scheffler from which the −1/0 level is found to be near the CBE. [31] Including the shift, $q\Delta_{VBE}$, the formation energies in the dilute limit are 1.86 eV for the 0 charge state and 3.31 eV for the −1 charge state (TABLE II). The result for the 0 charge state is in good agreement with the 1.93 eV obtained by Schultz and von Lilienfeld using the LDA. [34]

B. Thermal transitions between *EL2** and *EL2*

Experimental studies report that neutral *EL2* can be optically excited into neutral *EL2** at temperatures below 140 K. [29] Our DFT results are consistent with this report in that our formation energy for neutral *EL2* is 0.37 eV lower than our formation energy for neutral *EL2** (i.e. *EL2** is metastable with respect to *EL2*). In semi-insulating GaAs, it is further observed that neutral *EL2** transforms to *EL2* with an activation energy of 0.34 eV, [29] while in *n*-type GaAs, −1 *EL2** transforms to *EL2* with a lower activation energy of 0.075 eV, emitting an electron to the conduction band. [33]

In addition to our calculations for *EL*2 and *EL*2*, we used the dimer method [38] to determine the saddle-points for transitions between *EL*2* and *EL*2 in the 0 and −1 charge states. The saddle-point calculations were performed using the same supercell sizes and sampling meshes used for stable and metastable *EL*2 and *EL*2*. In Fig. 3, we plot the −1/0 levels of the saddle-points and cubic-spline fits of the bounds vs. inverse supercell size. Since the levels are between the lower and upper bounds and do not follow either bound, we concluded that −1 and 0 are well-localized defect charge states. However, since the levels are above Δ_{KS}, the added electron in the −1 charge state will be partially delocalized in bulk conduction-band states. We estimated the bulk charge to be 2, 6, and 8% in the 216-, 512-, and 1000-atom supercells, and based on this we proceeded to process the results using the procedures described in Section II.C. The dashed line in Fig. 3 is the supercell-size dependence of the defect level, $\Delta^{D,ssd}(-1/0,L)$, from which we obtain a dilute limit 0.90 eV above the VBE. After shifting the VBE by Δ_{VBE}, the −1/0 level is 1.31 eV above the VBE and thus within the measured band gap. The dilute limits of the formation energies (including the $q\Delta_{VBE}$ shift) are 2.07 eV for the 0 charge state and 3.36 eV for the −1 charge state. The corresponding formation energies of *EL2** are 1.86 and 3.31 eV. Thus, the activation energies for transitions from *EL2** to *EL2* are 0.21 eV in the 0 charge state and 0.05 eV in the −1 charge state.

Our result for the 0 charge state is 0.13 eV lower than the measured activation energy (0.34 eV) for the 0 charge state, [29] and our result for the −1 charge state is 0.025 eV lower than the measured activation energy (0.075 eV) for the −1 charge state. [33] In addition, our result for the 0 charge state is 0.02 eV higher than the activation energy obtained by Schultz and von Lilienfeld using the LDA, [34] and our result for the −1 charge

state is close to the estimate of Dabrowski and Scheffler [29] (0 eV) based on an analysis of Kohn-Sham eigenvalues.

C. Ga antisite charge states and levels

Ga_{As} is the defect that results when a Ga atom substitutes for an As atom in GaAs. While Ga_{As} has not been studied as extensively as As_{Ga}, is it known from experiments to have T_d symmetry, three charge states (–2, –1, 0), and two levels (–1/0, –2/–1) 0.077 and 0.230 eV above the VBE. [36, 37] In our study of T_d Ga_{As} we considered the three observed charge states plus four additional candidates (–3, +1, +2, +3). In Fig. 4, we plot the levels and cubic-spline fits of the bounds vs. inverse supercell size. From an inspection of the plots, we eliminated the +3 and −3 charge states and concluded that −2, −1, 0, +1 and +2 are Ga_{As} charge states. The nearly constant separation of the −2/−1, −1/0, 0/+1, and +1/+2 levels from the lower bound (supercell-to-supercell variations ≤ 0.01 eV) indicates that some of these charge states may be hydrogenic states. Support for this comes from a simple electron-counting analysis of T_d Ga_{As} in which 4×2 = 8 electrons are needed to saturate the bonds between the Ga atom and its four near-neighbor Ga atoms, whereas 3 + 4×(3/4) = 6 are available in the neutral charge state. Thus, the Ga-Ga bonds will be saturated when Ga_{As} is in the –2 charge state, which will be localized and thus likely to attract and bind at least two holes. To investigate the possibility of hydrogenic states further, we performed a simple calculation of shallow hole states in GaAs.

Using a static dielectric constant of 12.8 [26] and a heavy hole mass of 0.51 m_o, [39] we calculated the binding energy of a hole in a hydrogenic defect state to a localized −2

defect charge to be 0.17 eV. Returning to the bounds analysis, we note that the separation between a given level and the lower bound is the energy gained by adding a hole to the defect instead of the valence band. For shallow defect states with energies near the VBE, we can think of this as the binding energy of the hole. For the −2/−1 level, the binding energies are between 0.22 and 0.23 eV for the three supercells (Fig. 4), which agree well with the result of our simple calculation. The corresponding hydrogenic radius is 6.7 Å, so it should be possible to represent such a state in the supercell sizes considered in our DFT study. In contrast, a hydrogenic defect state formed from the light hole band (m = 0.082 m_o [39]) would have a radius of 42 Å and a binding energy of only 0.03 eV, and we would not expect to be able to distinguish such a state from the VBE in our calculations. Thus, we consider only the heavy hole band in interpreting our data. As successive holes are added to the defect, they interact with both the attractive charge of the −2 defect and the repulsive charge of the other holes bound to it, the binding becomes weaker, the defect state becomes more extended, and the successive defect levels are closer to the VBE. Since we have not included spin-orbit coupling in our calculations, the heavy-hole band of GaAs is doubly degenerate at the VBE, two 1*s*-like hydrogenic defect states can be constructed from these bands, and each of these states can contain a spin-up and a spin-down electron. Thus, we should be able to accommodate up to four holes in these states to produce charge states ranging from −1 to +2. Our DFT −2/−1, −1/0, 0/+1, and +1/+2 levels display successively smaller binding energies, consistent with this simple analysis.

When a fifth hole is added to a localized −2 defect charge in GaAs (treated without spin-orbit coupling), it can no longer be accommodated in a 1*s*-like hydrogenic

defect states, and we also might expect the repulsive interaction with the other holes to overwhelm the attractive interaction with the −2 defect. Our DFT results for the +2/+3 level of Ga_{As} are consistent with this. In the 216-atom supercell, our calculated +2/+3 defect level lies below the lower bound indicating that the additional hole does not have enough volume to completely avoid the repulsive region near the defect. In the larger supercells, the additional hole can more effectively avoid the repulsive interaction, and the calculated defect levels coincide more closely with the lower bound. If spin-orbit coupling was included in our calculations, there would only be a single heavy hole band at the VBE, and only two holes could be accommodated in 1*s*-like hydrogenic defect states. Thus, our results for the +1 and +2 charge states of GaAs would change, and it would not be surprising to find that the third and fourth hole would then be unbound with the 0/+1, and +1/+2 levels behaving like our calculated +2/+3 levels.

We note that the possibility of interpreting the Ga_{As} levels as shallow levels was considered by Schultz and von Lilienfeld.[34] However, a comparison of the levels to the bounds is needed to recognize the similarity in the energies to add a hole to the defect and to bulk GaAs. If we did not perform this analysis and simply used Makov-Payne fits to obtain the dilute limits of the −2/−1 and −1/0 levels as though the −1 and 0 charge states were highly localized, we would have obtained levels 0.33 eV and 0.16 eV above the VBE. After shifting the VBE by Δ_{VBE}, the −2/−1 level would be 0.74 eV above the VBE and the −1/0 level would be 0.56 eV above the VBE. These values are nearly identical to the 0.74 and 0.55 eV obtained by Schultz and von Lilienfeld[34] using the LDA, and are slightly higher than the 0.61 and 0.26 eV found by Chroneos *et al.*[35] They are also close to the 0.75 and 0.45 eV found by Komsa and Pasquarello,[40] who used a hybrid functional

and corrected their formation energies for spurious electrostatic interactions. In contrast, the bounds analysis (Fig. 4) shows that the levels are separated from the lower bound by small and essentially constant binding energies (0.22 - 0.23 eV for the −2/−1 level and 0.15 - 0.16 eV for the −1/0 level). The large separations between these levels and the VBE noted above thus arise from the Makov-Payne fits, used to remove electrostatic interactions between periodically repeated supercells, and the subsequent shift of the DFT VBE. These procedures assume highly-localized charge states, and if our interpretation of the charge states as weakly localized is correct, these assumptions and are not satisfied and the use of these procedures is not justified. Instead, we believe that if calculations for larger supercells were performed, these levels would continue to follow the lower bound with essentially the same binding energies. Furthermore, since hydrogenic defect states are constructed from VBE states, we propose that these levels should be shifted relative to the VBE. Based on the binding energies in the 1000-atom supercell, we therefore predict that Ga_{As} has a −2/−1 level 0.23 eV above the VBE and a −1/0 level 0.16 eV above the VBE.

Experimental studies indicate that Ga_{As} forms a double acceptor with levels 0.230 eV and 0.077 eV above the VBE. [36, 37] Our result for the −2/−1 level (0.23 eV) agrees exceptionally well with measurements (TABLE I), whereas the agreement is not as good for the −1/0 level (0.16 eV). One possible reason is that we neglected spin-orbit coupling in our DFT calculations. As discussed above, this results in degenerate 1*s*-like hydrogenic defect states, and this artificial degeneracy may reduce the Coulomb interaction when two holes are added to the −2 charged defect. In reality, the second hole must occupy the same state as the first hole (with the opposite spin), which likely will result in a larger

Coulomb interaction and thus a smaller binding energy for the second hole. Based on the formation energy of the 0 charge state in the 1000-atom supercell (3.16 eV) and the levels given above, we estimate the formation energy of the −1 charge state to be 3.32 eV and the formation energy of the −2 charge state to be 3.55 eV in the dilute limit (TABLE II). Our result for the 0 charge state is in good agreement with the 3.24 eV found by Schultz and von Lilienfeld using the LDA. [34]

IV. CONCLUSIONS

We have used a recently developed bounds-analysis approach to help interpret the results from DFT calculations for As_{Ga} and Ga_{As} defects in GaAs. The analysis correctly identified the charge states and levels of As_{Ga}, including the −1/0 level of the metastable state, which is observed to be close to the CBE. For Ga_{As}, the bounds analysis indicated the presence of hydrogenic states and a simple calculation of hydrogenic hole states in GaAs confirmed that the −1 and 0 charge states are hole states weakly bound to a localized −2 charge state. This insight precluded processing the −2/−1 and −1/0 levels using standard procedures and thereby produced good agreement with measurements.

ACKNOWLEDGMENT

This work was performed, in part, at the Center for Integrated Nanotechnologies, a U.S. Department of Energy, Office of Basic Energy Sciences user facility. Sandia

National Laboratories is a multi-program laboratory managed and operated by Sandia Corporation, a wholly owned subsidiary of Lockheed Martin Corporation, for the U.S. Department of Energy's National Nuclear Security Administration under contract DE-AC04-94AL85000. The authors wish to thank S. R. Lee and W. R. Wampler at Sandia National Laboratories for helpful discussions.

References

[1] W. Kohn and L. J. Sham, Phys. Rev. **140**, A1133 (1965).

[2] See for example: D. M. Ceperley and B. J. Alder, Phys. Rev. Lett. **45**, 566 (1980); J. P. Perdew and Y. Wang, Phys. Rev. B **45**, 13244 (1992).

[3] See for example: J. P. Perdew, K. Burke and M. Ernzerhof, Phys. Rev. Lett. **77**, 3865 (1996).

[4] See for example: S. M. Myers, P. J. Cooper, and W. R. Wampler, J. Appl. Phys. 104, 044507 (2008).

[5] N. A. Modine, A. F. Wright, and S. R. Lee, Computational Materials Science, **92**, 431 (2014).

[6] See http://dft.sandia.gov/socorro.

[7] J. Ihm, A. Zunger, and M. L. Cohen, J. Phys. C **12**, 4409 (1979).

[8] D. R. Hamann, M. Schülter, and C. Chiang, Phys. Rev. Lett. **43**, 1494 (1979).

[9] http://www.fhi-berlin.mpg.de/th/fhi98PP/. Three electrons were treated as valence ($4s_2$ and $4p_1$) in Ga and five electrons ($4s_2$ and $4p_3$) in As. Cutoff radii of 1.10, 1.30, and 2.25 Bohr were used for the *s*, *p*, and *d* channels of Ga and 1.00, 1.18, and 1.80 Bohr were used for As. Non-linear core corrections [S. G. Louie, S. Froyen, and M. L. Cohen, Phys. Rev. B **26**, 1738 (1982)] were included for both atom types with partial core charge radii of 1.20 and 1.00 Bohr for Ga and As, respectively.

[10] L. Kleinman and D. M. Bylander, Phys. Rev. Lett. **48**, 1445 (1982). Projectors were constructed using the *s* semilocal NCP as the local potential.

[11] H. J. Monkhorst and J. D. Pack, Phys. Rev. B **13**, 5188 (1976).

[12] F. D. Murnaghan, Proc. Natl. Acad. Sci. U.S.A. **30**, 244 (1944).

[13] J. B. Mullin, B. W. Straughan, C. M. H. Driscoll, and A. F. W. Willoughby, Inst. Phys. Conf. Ser. **24**, 275 (1975).

[14] J. S. Blakemore, J. Appl. Phys. **53**, R123 (1982).

[15] B. J. Skromme and G. E. Stillman, Phys. Rev. B **29**, 1982 (1984).

[16] E. A. Brandes, in *Smithells Metals Reference Book* (Butterworths, London, 1983).

[17] J. Donohue, *The Structures of the Elements* (Wiley, New York, 1974).

[18] Y. Bar-Yam and J. D. Joannopoulos, Phys. Rev. B **30**, 1844 (1984).

[19] A. Alkauskas, P. Broqvist, and A. Pasquarello, Phys. Stat. Sol. B **248**, 775 (2011).

[20] C. D. Latham, M. Alatalo, R. M. Nieminen, R. Jones, S. Oberg, and P. R. Bridden, Phys. Rev. B **72**, 235205 (2005).

[21] For another example of this type of plot, see H.-P. Komsa, T. T. Rantala, and A. Pasquarello, Phys. Rev. B **86**, 045112 (2012). The bounds-analysis approach is analogous to their approach, differing in that whereas their approach employs the defect and the band-edge eigenvalues, the bounds-analysis approach uses the defect levels and bounds on defect levels.

[22] S. B. Zhang and J. E. Northrup, Phys. Rev. Lett. **67**, 2339 (1991).

[23] C. G. Van de Walle, D. B. Laks, G. F. Neumark, and S. T. Pantelides, Phys. Rev. B **47**, 9425 (1993).

[24] C. Freysoldt, B. Grabowski, T. Hickel, J. Neugebauer, G. Kresse, A. Janotti, and C. G. Van de Walle, Rev. Mod. Phys. **86**, 253 (2014).

[25] G. Makov and M.C. Payne, Phys. Rev. B **51**, 4014 (1995).

[26] J. S. Blakemore, J. Appl. Phys. **53**, R123 (1982).

[27] A. Resende, R. Jones, S. Öberg, and P. R. Briddon, Phys. Rev. Lett. **82**, 2111 (1999); J. Coutinho, S. Öberg, V. J. B. Torres, M. Barroso, R. Jones, and P. R. Briddon, Phys. Rev. B **73**, 235213 (2006).

[28] H.-P. Komsa and A. Pasquarello, Phys. Rev. B, **84**, 075207, (2011).

[29] For a thorough discussion of experimental and theoretical investigations of As_{Ga} see J. Dabrowski and M. Scheffler, Phys. Rev. B. **40**, 10391 (1989) and references therein.

[30] J. Lagowski, D. G. Lin, T. –P. Chen, M. Skonwronski, and H. C. Gates, Appl. Phys. Lett. **6,** 929 (1985).

[31] J. Dabrowski and M. Scheffler, Phys. Rev. Lett. **60**, 2183 (1988)

[32] D. J. Chadi and K. J. Chang, Phys. Rev. Lett. **60**, 2187 (1988).

[33] P. Dreszer and M. Baj, J. Appl. Phys. **70**, 2679 (1991).

[34] P. A. Schultz and O. A. von Lilienfeld, Modelling Simul. Mater. Sci. Eng. **17**, 084007 (2009).

[35] A. Chroneos, H. A. Tahini, U. Schwingenschlögl, and R. W. Grimes, J. Appl. Phys., **116**, 023505, (2014).

[36] Phil Won Yu, W. C. Mitchel, M. G. Mier, S. S. Li, and W. L. Wang, Appl. Phys. Lett. **41**, 532 (1982).

[37] J. C. Bourgoin, H. J. Bardeleben, and D. Stiévenard, J. Appl. Phys. **64**, R65 (1988), and references therein.

[38] G. Henkelman and H. Jonsson, J. Chem. Phys. **111**, 7010 (1999).

[39] http://www.ioffe.rssi.ru/SVA/NSM/Semicond/GaAs/basic.html.

[40] H-P. Komsa and A. Pasquarello, J. Phys.: Condens. Matter **24**, 045801 (2012).

TABLE I. Comparison of our DFT defect levels at the dilute limit with experiments. The levels are given in eV relative to either the valence-band edge (VBE) or the conduction-band edge (CBE).

Defect and Level	DFT	Expt.
EL2 As_{Ga} 0/+1	VBE + 0.76	VBE + 0.77 [a]
+1/+2	VBE + 0.54 [*]	VBE + 0.54 [a]
*EL2** As_{Ga} −1/0	CBE − 0.06	CBE + 0.016 [b]
Ga_{As} −2/−1	VBE + 0.23	VBE + 0.230 [c]
−1/0	VBE + 0.16	VBE + 0.077 [c]

[*] Used as a marker to obtain the shift of the DFT VBE.
[a] Ref. 30
[b] Ref. 33
[c] Refs. 36 and 37

TABLE II. Formation energies at the dilute limit in eV.

Defect and Charge State	Formation energy
*EL*2 As_{Ga} 0	1.49
+1	0.73
	0.19
*EL*2* As_{Ga} −1	3.31
0	1.86
Ga_{As} −2	3.55
−1	3.32
0	3.16

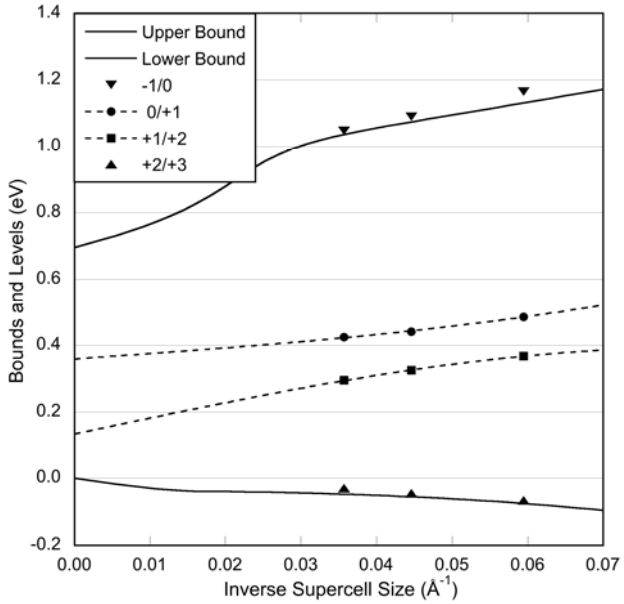

Figure 1. Bounds and *EL*2 levels vs. inverse supercell size (1/*L)*. The solid lines are cubic-spline fits of the bounds, $\Delta^{B,fit}(-1,L)$ and $\Delta^{B,fit}(+1,L)$. The symbols are DFT levels, $\Delta^{D}(q-1/q,L)$, from 216-, 512- and 1000-atom supercells. The dashed lines are the supercell-size dependences of the DFT defect levels, $\Delta^{D,ssd}(q-1/q,L)$, identified in the bounds-analysis.

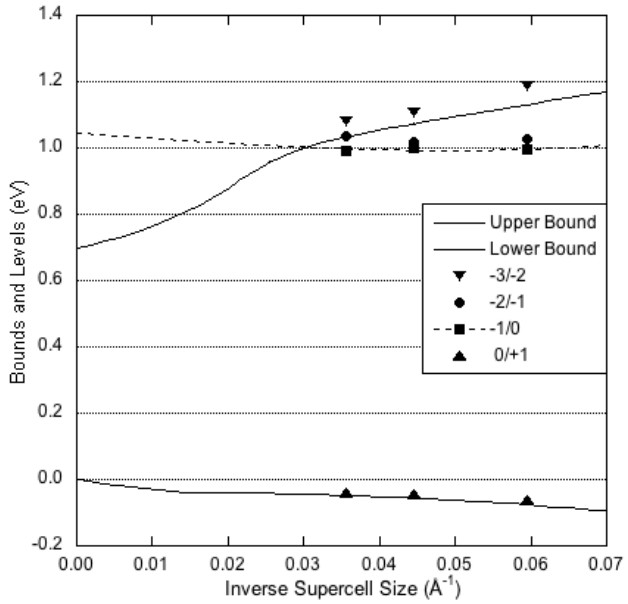

Figure 2. Bounds and *EL*2* levels vs. inverse supercell size (1/*L*). The solid lines are cubic-spline fits of the bounds, $\Delta^{B,fit}(-1,L)$ and $\Delta^{B,fit}(+1,L)$. The symbols are DFT levels, $\Delta^{D}(q-1/q,L)$, from 216-, 512- and 1000-atom supercells. The dashed line is the supercell-size dependence of the DFT defect level, $\Delta^{D,ssd}(-1/0,L)$, identified in the bounds-analysis.

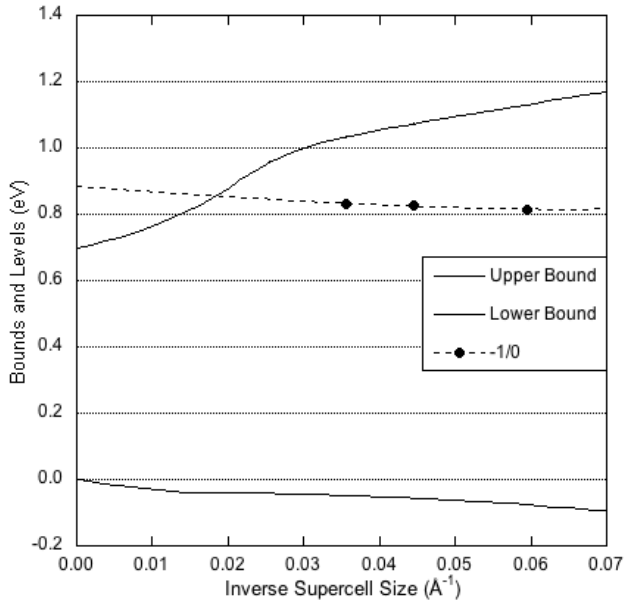

Figure 3. Bounds and saddle-point level vs. inverse supercell size ($1/L$). The solid lines are cubic-spline fits of the bounds, $\Delta^{B,fit}(-1,L)$ and $\Delta^{B,fit}(+1,L)$. The symbols are DFT levels, $\Delta^{D}(q-1/q,L)$, from 216-, 512- and 1000-atom supercells. The dashed lines are the supercell-size dependences of the DFT defect levels, $\Delta^{D,ssd}(q-1/q,L)$, identified in the bounds-analysis.

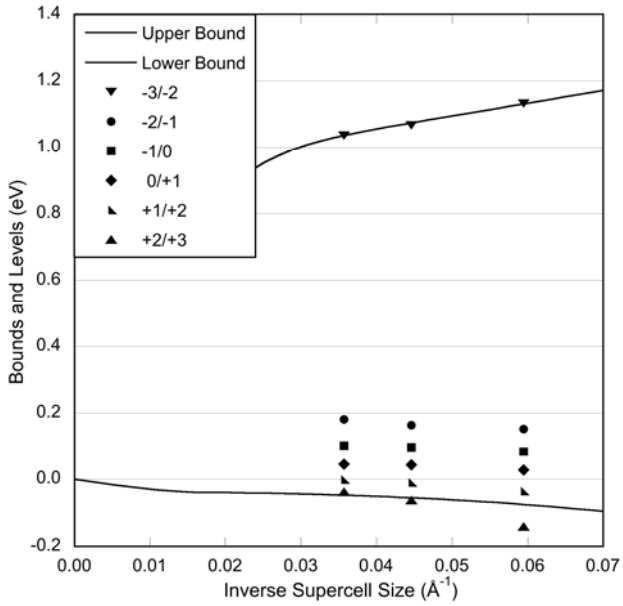

Figure 4. Bounds and Ga_{As} levels vs. inverse supercell size, $1/L$. The symbols are DFT levels, $\Delta^D\left(q-1/q,L\right)$, from 216-, 512- and 1000-atom supercells.